IOPscience iopscience.iop.org

Home Search Collections Journals About Contact us My IOPscience

Effects of spin–orbit coupling on the conductance of molecules contacted with gold electrodes

This article has been downloaded from IOPscience. Please scroll down to see the full text article.

2009 J. Phys.: Condens. Matter 21 335301

(http://iopscience.iop.org/0953-8984/21/33/335301)

View the table of contents for this issue, or go to the journal homepage for more

Download details:
IP Address: 129.252.86.83
The article was downloaded on 29/05/2010 at 20:44

Please note that terms and conditions apply.

J. Phys.: Condens. Matter **21** (2009) 335301 (9pp) doi:10.1088/0953-8984/21/33/335301

Effects of spin–orbit coupling on the conductance of molecules contacted with gold electrodes

Ruoxing Zhang[1], Guohui Ma[1], Rui Li[1], Zekan Qian[1], Ziyong Shen[1], Xingyu Zhao[1], Shimin Hou[1,3] and Stefano Sanvito[2]

[1] Key Laboratory for the Physics and Chemistry of Nanodevices, Department of Electronics, Peking University, Beijing 100871, People's Republic of China
[2] School of Physics and CRANN, Trinity College, Dublin 2, Republic of Ireland

E-mail: smhou@pku.edu.cn

Received 22 May 2009
Published 28 July 2009
Online at stacks.iop.org/JPhysCM/21/335301

Abstract

The effects of spin–orbit coupling on the conductance of molecular devices made with Au electrodes are investigated using a fully self-consistent *ab initio* approach, which combines the non-equilibrium Green's function formalism with density functional theory. In general, we find that the extent to which spin–orbit interaction affects the transport depends on the specific materials system investigated and on the dimensionality of the electrodes. For one-dimensional electrodes contacting benzene–dithiol molecules the spin–orbit coupling induces changes in the low-bias conductance up to about 20%. These originate mostly from changes in the electrode band structure. In contrast when three-dimensional electrodes are used, the bands near the Fermi level are only weakly modified by spin–orbit coupling and most of the variations are due to symmetry changes at the molecule–electrode interface. For this reason strongly coupled systems, such as Au atomic nanowires sandwiched between Au (100) surfaces and benzene–dithiol molecules bonded at the Au (111) hollow site, are rather insensitive to spin–orbit effects. In contrast, in junctions where the coupling between the molecule and the electrodes is weaker, as in the case of benzene–dithiol bonded to Au (111) at adatom positions, the transmission coefficient at the Fermi level can be modified by as much as 14%.

(Some figures in this article are in colour only in the electronic version)

1. Introduction

In recent years molecular devices have attracted continuously growing attention, and molecular electronics is now believed to be one of the most promising solutions for tackling the limitations of silicon-based microelectronic device miniaturization [1, 2]. Due to the high conductivity and chemical inertness, gold (Au) is widely used as the electrode material for constructing molecular devices. In order to make stable connections between the molecule and the gold electrodes, appropriate terminal groups such as thiol, pyridine and amine are often employed [3–7].

First-principles theoretical calculations are a powerful tool for the development of molecular electronics. They can guide the design of molecular devices and improve their performance. In particular they are useful in understanding the often controversial experiments. In some cases, for instance, there is no consensus on the experimentally measured single-molecule conductance, with values differing by more than two orders of magnitude reported for the same molecule [3–5, 8, 9]. At present, the most widely used theoretical approach combines the non-equilibrium Green's function (NEGF) formalism [10, 11] with density functional theory (DFT) [12, 13], that is, the NEGF + DFT approach [14–19]. Within the NEGF + DFT framework several research groups have developed a number of software packages for calculating electron transport in molecular devices, most of which are based on local orbital and pseudopotential implementations of DFT [17–19]. Since

[3] Author to whom any correspondence should be addressed.

 © 2009 IOP Publishing Ltd Printed in the UK

relativistic effects become more important with increasing atomic number, scalar relativistic (SR) corrections to the band structure of the Au electrodes have been included via the pseudopotentials. However, so far, these neglect spin–orbit (SO) interaction completely.

Such deficiencies of many current transport calculations contrasts the common belief that SO coupling should in principle always be included when computing properties of molecules and solids containing heavy elements. For example, SO interaction significantly affects the stability of the D_{3h} isomer of Au_3 [20], and it is also found to play an important role in the band structures of one-dimensional (1D), two-dimensional (2D) and three-dimensional (3D) Au [21]. Furthermore, by comparing the fully relativistic (here we denote as fully relativistic—FR—calculations explicitly including SO interaction) and the SR transmission coefficients of Pt monatomic nanowires, it was demonstrated that SO effects could be quite important in predicting the ballistic conductance of nanojunctions [22]. From this analysis it emerges that the investigation of electron transport through molecular devices made with Au electrodes in the presence of SO interaction is an important question to be addressed.

It is well known that the steady-state current through a two-terminal molecular device is influenced by the quantum nature of the molecule, the geometry-dependent molecule–electrode coupling and the electronic properties of the electrodes near the Fermi level [23]. Therefore, although the SO interaction in individual organic molecules composed of light elements (H, C, N and S) is expected to be tiny, SO interaction might still have a significant influence on the conductance of molecular junctions made with Au electrodes. In fact both the band structures of Au electrodes and the interaction between the electrodes and the molecule can be largely modified by SO coupling. Importantly, its effect will be magnified in low-dimensional electrodes such as Au monatomic chains, where the Fermi surface is formed by electronic states with a very well-defined orbital symmetry. Note that, low-dimensional electrodes may become important for future integrated circuits based on molecular devices [24–30], since their size is comparable to that of the molecules embedded in the device.

In the following sections we will first introduce the main theoretical tool for our investigation and then we present our results. We will start by discussing the SO effects over the band structure of 1D and 3D Au electrodes, and then we will proceed in investigating a number of two-probe devices. We will begin by looking at Au quantum point contacts, for which a substantial amount of experimental data is available. Then we will move to benzene–dithiol (BDT) molecules sandwiched between Au monatomic chains, and finally we will consider the same molecule now attached to Au (111)-terminated three-dimensional electrodes. In this last case we will consider three different bonding geometries, namely: (1) BDT attached to the Au (111) hollow site, (2) an asymmetric geometry where BDT is attached to the hollow site of one electrode and to an adatom of the other, and (3) a BDT molecule attached to adatoms of both the electrodes.

2. Computational method

The conductance at zero bias is calculated by using a fully self-consistent NEGF + DFT approach, which has been extensively described elsewhere [14, 19, 31]. The retarded Green's function of the extended molecule, which comprises the molecule itself and several atomic layers of its neighboring electrodes, is defined as

$$G^{\mathrm{R}}(E) = \left[(E + \mathrm{i}\eta)\, S - H - \sum\nolimits_{\mathrm{L}} - \sum\nolimits_{\mathrm{R}}\right]^{-1}, \quad \eta \to 0^{+} \tag{1}$$

where H and S are respectively the Hamiltonian and the overlap matrix of the extended molecule, and the self-energy matrices Σ_{L} and Σ_{R} incorporate the effect of the two semi-infinite electrodes. Due to the analytic properties of the retarded Green's function G^{R}, the density matrix of the extended molecule can be efficiently calculated by integrating the Green's function along a contour in the upper half energy plane [31]:

$$D = \frac{\mathrm{i}}{2\pi}\left(\int_C G(z) f(z - E_{\mathrm{F}})\,\mathrm{d}z - 2\pi \mathrm{i} kT \sum_{z_n} G(z_n)\right) + \text{c.c.}, \tag{2}$$

where E_{F} is the Fermi energy of the electrode, T is the temperature (300 K in our calculations) and $z_n = E_{\mathrm{F}} + \mathrm{i}(2n + 1)\pi \mathrm{kT}$ are the poles of the Fermi distribution $f(E - E_{\mathrm{F}})$. Then, the Kohn–Sham Hamiltonian matrix of the extended molecule is calculated from the density matrix of equation (2). Both the electrostatic and the exchange–correlation corrections are included [14], so that the influence of the charge distribution of the electrodes is considered completely. By iterating the equations (1) and (2) with the newly constructed Kohn–Sham Hamiltonian until self-consistency is reached, we can obtain a non-equilibrium self-consistent final Kohn–Sham Hamiltonian matrix and the Green's function. This is then used for calculating the transport. Thus the density of states (DOS) and the transmission coefficient as a function of energy are calculated as

$$\mathrm{DOS}(E) = \frac{\mathrm{i}}{2\pi}\mathrm{trace}((G^{\mathrm{R}} - G^{\mathrm{A}})S), \tag{3}$$

$$T(E) = \mathrm{trace}(\Gamma_{\mathrm{L}} G^{\mathrm{R}} \Gamma_{\mathrm{R}} G^{\mathrm{A}}), \tag{4}$$

where $\Gamma_{\mathrm{L,R}} = \mathrm{i}(\Sigma_{\mathrm{L,R}} - \Sigma^{+}_{\mathrm{L,R}})$ are the broadening function matrices of the electrodes. The low-bias molecular conductance is related to the transmission coefficient at the Fermi level by $G = (e^2/h)T(E_{\mathrm{F}})$. In the case of translational invariance along the direction perpendicular to the transport the transmission coefficient is k-dependent and must be averaged over the transverse 2D Brillouin zone [19].

A development version [32] of the SIESTA package [33], in which SO interaction in DFT is included via the pseudopotentials obtained from a relativistic *ab initio* calculation, is employed for both the FR and SR case. We use the Perdew–Zunger version of the local spin density approximation (LSDA) for the exchange and correlation potential [34], although LDA with self-interaction corrections (SIC) is more suitable for NEGF + DFT calculations [35–37].

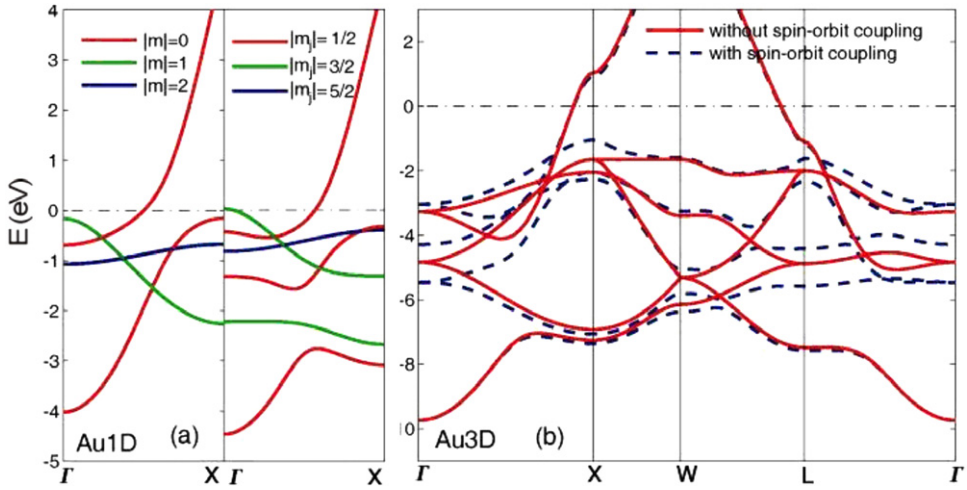

Figure 1. SR and FR band structures of 1D and 3D fcc Au: (a) energy bands for the 1D Au monatomic chain calculated both with and without considering SO interaction; (b) energy bands for bulk fcc Au. The Fermi energy is set to zero.

Unfortunately at present there is no non-collinear formulation of the SIC, which therefore cannot be used together with SO coupling. Both the scalar and the SO part of the pseudopotentials for the atomic cores are generated by using the well-known procedure introduced by Kleinman and Bylander [38–40]. The wavefunctions of the valence electrons are expanded in terms of a finite range numerical basis set. By means of extensive optimization, a user-defined double ζ plus polarization (DZP) basis set is constructed for the H, C and S atoms, and a single ζ plus polarization (SZP) basis set is used for Au. The on-site approximation to the SO matrix elements is employed to reduce the computational effort, and it is justified by the fact that the radial part of the SO pseudopotential is very short-ranged. The details of the implementation in the SIESTA code can be found in [32]. The transport is calculated using a development version of the Smeagol package [19] including SO interaction.

3. Results and discussion

3.1. Band structures of Au

First we examine the band structures of Au in both its bulk 3D fcc structure and in the form of a 1D free-standing linear monatomic chain, where the Au–Au bond lengths are taken to be 2.884 Å and 2.733 Å respectively [41]. The band structure for the 1D chain is shown in figure 1(a) (note that, as a convention, we align the chain along the z-direction). When SO interaction is neglected, both the orbital angular momentum and spin are good quantum numbers, thus the bands can be labeled by the integer eigenvalues m of the z-component of the orbital angular momentum L_z. Because of the restricted space symmetry, only two atomic orbitals with the same value of m along the chain axis can interact with each other and form a band. The $m = 0$ bands (red) are composed of the 6s and $5d_{z^2}$ atomic orbitals, and the band energy increases when going from Γ to X. In addition to the spin degeneracy, the $|m| = 1$ bands (green) are doubly degenerate. They are composed of the orthogonal orbitals $5d_{xz}$ and $5d_{yz}$ respectively and the band energy decreases from Γ to X. Among all of the 1D energy bands, the $|m| = 2$ bands (blue) are the narrowest ones due to the smallest overlap of the $5d_{xy}$ or $5d_{x^2-y^2}$ atomic orbitals between two neighboring atoms. These are also doubly degenerate and the energy increases when going from Γ to X. To summarize, when SO interaction is neglected, there is only one $m = 0$ band crossing the Fermi energy, so that there are only two spin-degenerate conduction channels that can contribute to the zero-bias conductance.

When the SO interaction is switched on, the energy bands can no longer be distinguished by the magnetic quantum number m, since neither the orbital angular momentum nor the spin are good quantum numbers. Thus the energy bands are labeled by the half-integer eigenvalues m_j of the z-component of the total angular momentum J_z. As we can see from figure 1(a), there are now three $|m_j| = 1/2$ bands (red), two $|m_j| = 3/2$ bands (green) and one $|m_j| = 5/2$ band (blue). All of the six energy bands are doubly degenerate due to time-reversal symmetry. The $m_j = 1/2$ ones are composed of three orbitals with different symmetry, namely the 6s and $5d_{z^2}$ for spin-up and the $5d_{xz} + i5d_{yz}$ for spin-down. In contrast the $m_j = -1/2$ band is formed from 6s and $5d_{z^2}$ orbitals for spin-down and from $5d_{xz} - i5d_{yz}$ for spin-up. Similarly, the orbital composition for the $m_j = 3/2$ band is $5d_{xz} + i5d_{yz}$ for spin-up and $5d_{x^2-y^2} + i5d_{xy}$ for spin-down, while that of the $m_j = -3/2$ band is $5d_{xz} - i5d_{yz}$ for spin-down and $5d_{x^2-y^2} - i5d_{xy}$ for spin-up. Finally, the $m_j = 5/2$ band is formed only by the orbitals $5d_{x^2-y^2} + i5d_{xy}$ for spin-up, while the $m_j = -5/2$ one is formed only by the $5d_{x^2-y^2} - i5d_{xy}$ orbital for spin-down.

Since the conductance of a molecular device is critically dependent on the band structures of the electrodes near the Fermi level, we now focus our attention on the difference between the SR and FR energy bands near E_F. A close look at our results for the Au 1D monatomic chain shows that SO coupling increases the number of conduction channels at the Fermi level from two for the SR case to four for the FR

case, since now the $|m_j| = 3/2$ band touches the Fermi level near Γ. Furthermore, in the SR case the band crossing E_F is composed of only the 6s and $5d_{z^2}$ atomic orbitals, while in the FR case the two bands crossing E_F are composed of 6s and all the five 5d symmetries. In addition, at about 2 eV below E_F, there is a 1 eV energy gap for the FR case, so that we expect the transmission coefficient of a molecular device with Au monatomic chain electrodes to vanish in that energy range.

The SR and FR band structure of 3D fcc Au are shown next in figure 1(b). As one can see, also in this case there are significant differences between the SR and FR bands, in particular well below E_F, where the contribution of the filled 5d shell to the DOS is most relevant. However, when compared to the 1D case, the changes at E_F appear minimal, due to the predominantly s-character of the Au Fermi surface. Our calculations are fully consistent with previous results reported in the literature [21, 42].

3.2. Transport property: Au quantum point contacts

In the previous section we have shown that the number of transport channels at the Fermi level in 1D chains increases from 2 to 4 when the SO interaction is switched on. This seems to pose an intriguing puzzle. In fact the overwhelming majority of quantum point contact measurements report a ballistic conductance for Au breaking junctions before the rupture point of $2G_0$ (here we adopt the definition $G_0 = e^2/h$) [6, 25, 26], i.e. they are compatible with two scattering channels at the Fermi level (one spin-degenerate scattering channel). In order to understand this apparent disagreement we investigate the transport through a Au point contact model in which a 3-atom-long Au monatomic chain is sandwiched in between Au [100] electrodes formed in the shape of a pyramid (see figure 2(a)). This model is sufficiently realistic. In fact, although freely suspended gold monatomic chains up to seven or eight atoms long can be created, the probability for the formation of chains of two and three atoms is actually much larger [26], and therefore this is one of the most probable configurations to dominate the experimental conductance histograms.

The transmission coefficients as a function of energy calculated either with or without SO coupling are presented in figure 2(b). In the SR case there is a large transmission plateau at $T \sim 2$ around and above the Fermi level. This means that the low-bias conductance of $G = 2G_0$ is stable against fluctuations of the position of E_F, in good agreement with experiments. The transmission is then reduced at energies 0.38 eV below the Fermi level, it approaches zero at around $E_F - 0.66$ eV and then finally has a rapid increase reaching $T = 5.52$ at $E_F - 1.12$ eV. These low energy features are due to the interaction of the s-electrons with the d-manifold and are perfectly consistent with previously published work.

Importantly, the introduction of SO interaction does not change the transmission around E_F, indicating that SO does not play an important role in the low-bias transport properties of Au quantum point contacts. However, because of the SO coupling the first transmission peak below the Fermi level shifts from $E_F - 1.12$ eV to $E_F - 0.64$ eV and its amplitude reduces from 5.52 to 2.98. This already demonstrates that one should expect a low-bias conductance of $G = 2G_0$ in Au quantum point contacts, regardless of whether or not SO is considered. Again this is in good agreement with the experimental data [6, 25, 26].

In order to get a deeper insight into the conductance of Au quantum point contacts, we analyze the contributions to the transport of each of atomic orbitals forming the Au trimer sandwiched between the electrodes. This is realized by using our previously developed projection method based on scattering states [43]. The results are given in the figures 2(c) and (d) where we plot the orbital decomposition of the transmission coefficient as a function of the energy. In the SR case, Au atomic orbitals of 6s and $5d_{z^2}$ symmetry dominate the transmission around E_F, with a contribution to $T(E_F)$ of about 82.8%, and the remaining 17.2% originating from the $5d_{xz}$ and $5d_{yz}$ orbitals. This situation is reversed at the first transmission peak below the Fermi level (at $E_F - 1.12$ eV) where the $5d_{xz}$ and $5d_{yz}$ symmetries make the main contribution. The inclusion of SO coupling does not change the overall picture and the transmission around E_F is still dominated by Au atomic orbitals with $|m_j| = 1/2$, while the $|m_j| = 3/2$ provides only a tiny contribution. This result could not have been anticipated from a simple consideration of the bands of an infinite gold monatomic chain as shown in figure 1. Such a difference originates mainly from the shortness of the nanocontact—a gold trimer is far from infinite.

3.3. Transport property: BDT connected to two Au monatomic chains

We now turn our attention to study the effects of SO coupling on the conductance of molecular devices using Au electrodes. Although SO interaction has little effect on light elements, it can influence the charge distribution and the conductance of the molecule through the molecule–electrode coupling. BDT is chosen as the central molecule and it is attached to Au electrodes through the two S atoms of the thiol group. Our aim is simply to demonstrate the effects of SO coupling on the transport properties of molecular devices through a number of examples. We do not intend here to provide an exhaustive analysis of transport across BDT molecules connected to Au for which a rather extensive literature already exists [44–50].

With this in mind we first investigate the conductance of BDT connected to two semi-infinite 1D Au chains, here the Au–S–C bond angle is optimized to be 104.2° (see figure 3(d)). The transmission coefficients as a function of energy calculated with and without SO interaction are shown in figure 3(a). As one can notice, although the FR-calculated $T(E)$ above E_F is almost the same as that of the SR calculations, below E_F the two differ sensibly from each other. In the FR case, $T(E)$ shows a number of sharp transmission peaks and a large transmission gap at around −2 eV. More importantly, the transmission coefficient at E_F is increased from 1.88 for the SR case to 2.20 for the FR one. All of these differences can be traced back to the effects of SO coupling on the energy bands of the gold monatomic chain and to the molecule–electrode interaction. In the SR case, there is only one energy band crossing the Fermi level, so that the transmission coefficient

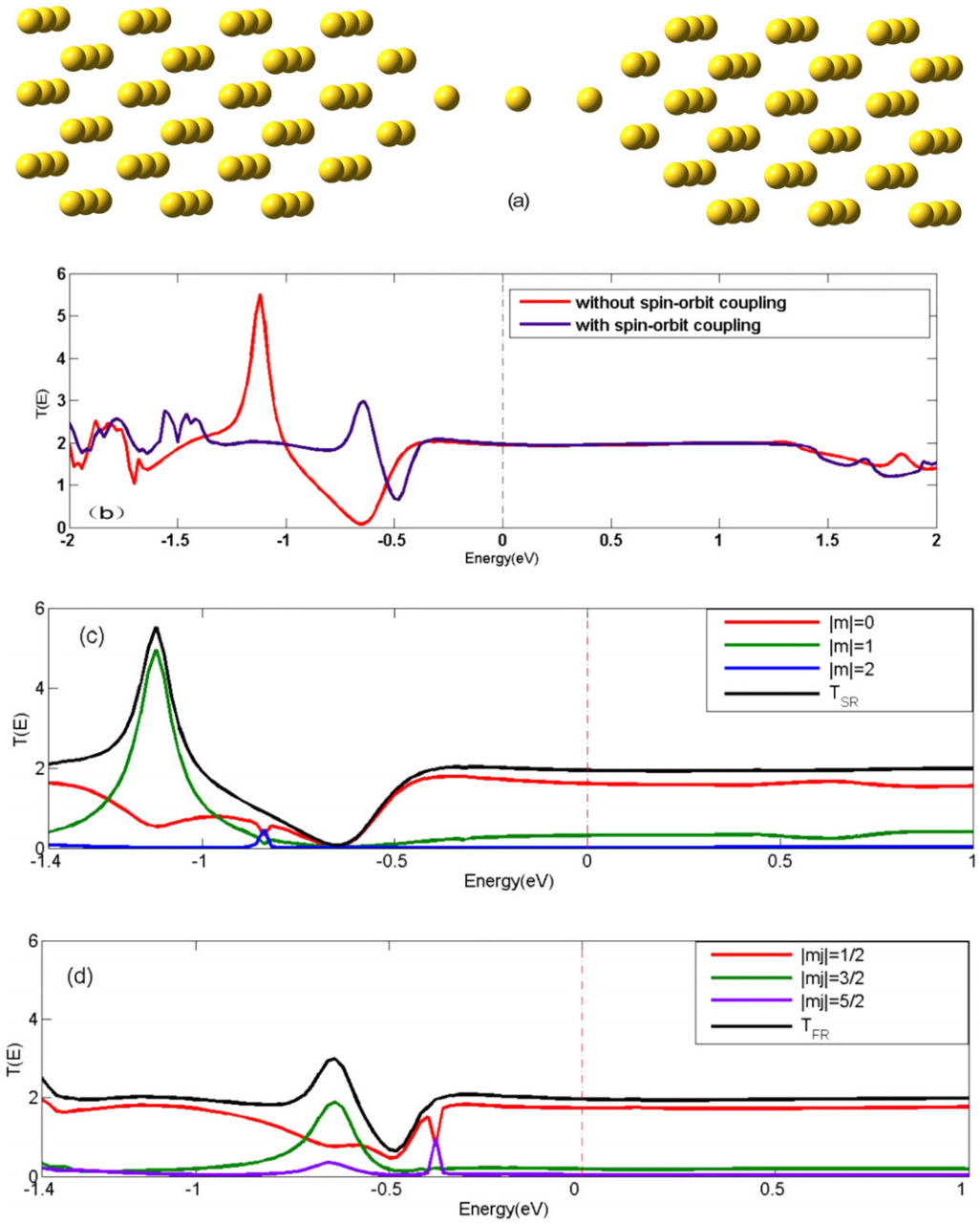

Figure 2. Au quantum point contact transport calculation: (a) geometrical structure of the model Au point contact investigated; (b) transmission coefficient as a function of energy calculated with and without SO coupling; (c) SR transmission coefficient projected onto the atomic orbitals of the gold trimer; (d) FR transmission coefficient projected onto the atomic orbitals of the gold trimer.

of the device at E_F is undoubtedly equal or less than two, since it is limited by the number of conduction channels in the electrodes. In contrast, in the FR case, there are two energy bands crossing the Fermi level so that the transmission coefficient can be as large as 4. Although the $T(E_F)$'s in the SR and FR case differ by only 17%, it is important to note that for the FR calculations $T(E_F)$ exceeds SR, the upper bound of 2 set by the number of scattering channels in the electrodes. Below E_F, the SO coupling causes band splitting and anti-crossing, which makes the transmission display a multitude of peaks near the band edges. In particular, for energies at around $E_F - 2$ eV there exists an energy gap opening due to SO coupling, thus no propagating states are present and the transmission also shows a gap. In contrast, above E_F the only energy band present is of s-character, the SO coupling does not affect it and the device transmission is not affected either.

Again in order to gain a deeper insight into the conductance mechanism, we project the transmission coefficient over the molecular orbitals of BDT. The contributions of the HOMO-2, HOMO and LUMO to the transmission for both the SR and FR calculations are shown in figures 3(b) and (c), respectively. Regardless of the SO interaction the HOMO-2 state dominates the transmission at E_F, while the LUMO contributes a transmission peak centered at about 4 eV above E_F. In contrast, the contribution of the HOMO is rather different in the SR and FR case, due to its particular orbital character. In fact,

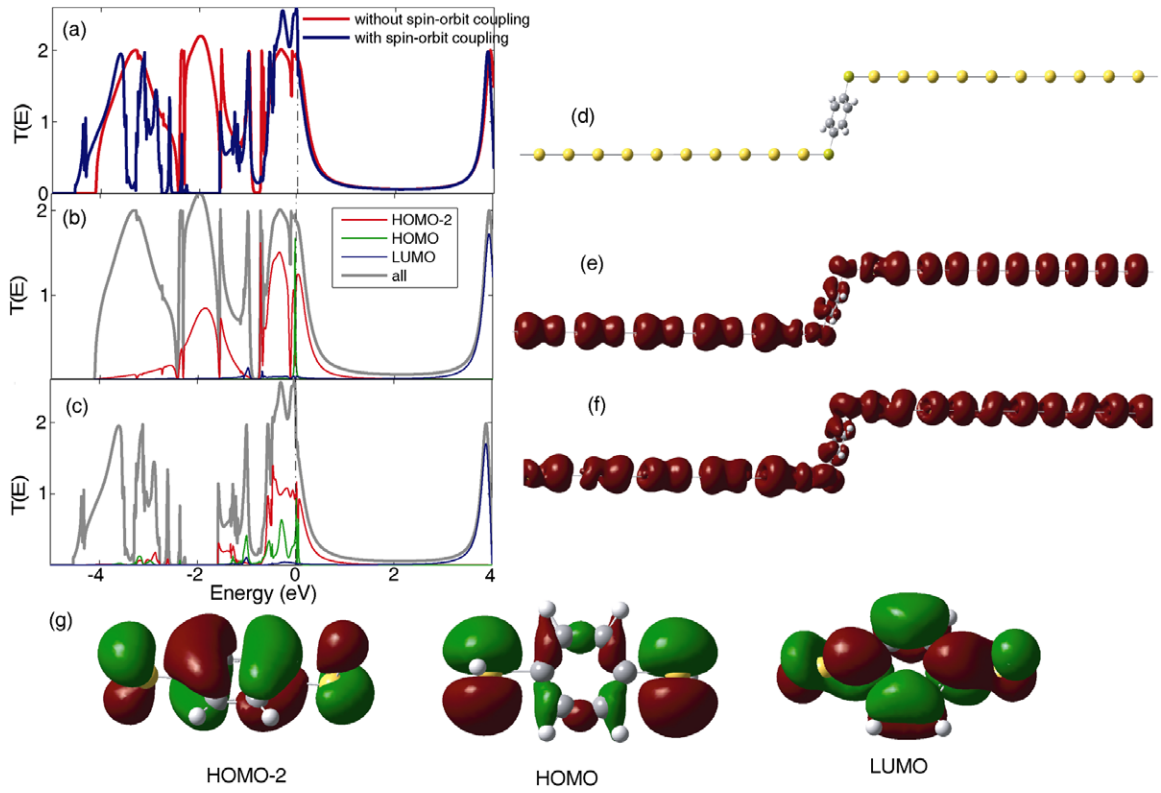

Figure 3. Transport calculations for a BDT molecule connected to two semi-infinite Au monatomic chains: (a) SR and FR transmission coefficients as a function of energy; (b) SR transmission coefficient projected onto the HOMO-2, HOMO and LUMO of the central molecule including the benzene backbone and the two anchoring S atoms; (c) FR transmission coefficient projected onto the HOMO-2, HOMO and LUMO; (d) optimized geometry of benzene connected to two semi-infinite Au monatomic chains; (e) scattering states at the Fermi level calculated without SO coupling; (f) scattering states at the Fermi level calculated with SO coupling; (g) charge density isosurfaces of the HOMO-2, HOMO and LUMO of the central molecule.

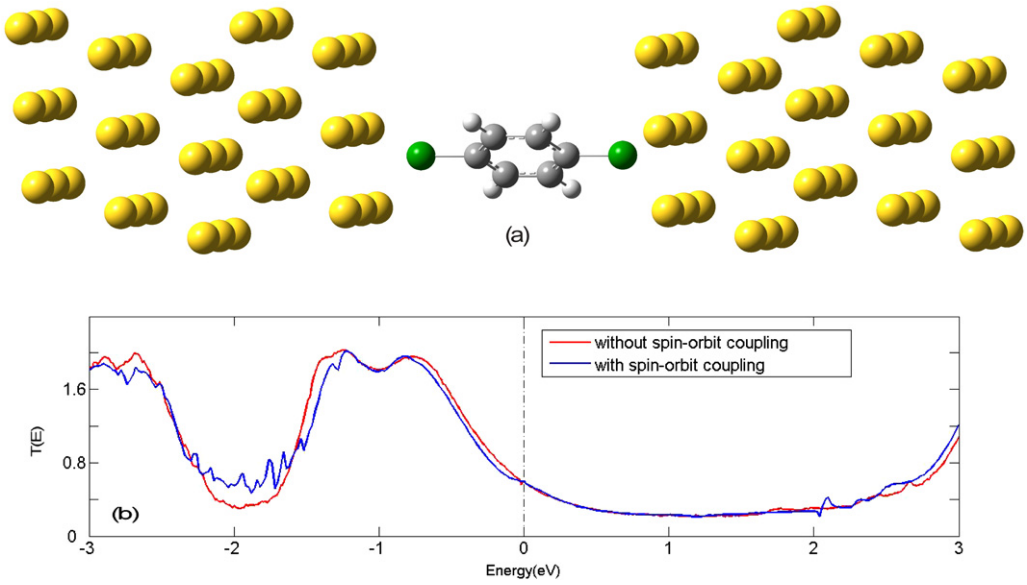

Figure 4. Transport calculations for a BDT molecule attached to two 3D Au electrodes at the Au (111) hollow site: (a) optimized geometry; (b) SR and FR transmission coefficients.

while (see figure 3(g)) both the HOMO-2 and the LUMO are π-type molecular orbitals, composed both of C and S p_z orbitals (the transport is along the z-axis), the HOMO is of σ-type and it is mainly composed of S p_y orbitals.

For SR calculations the scattering channels in the Au electrodes at E_F are composed of 6s and $5d_{z^2}$ atomic orbitals, which can interact strongly with the p_z orbitals of S. For this reason, the transmission coefficient at the Fermi level is mainly

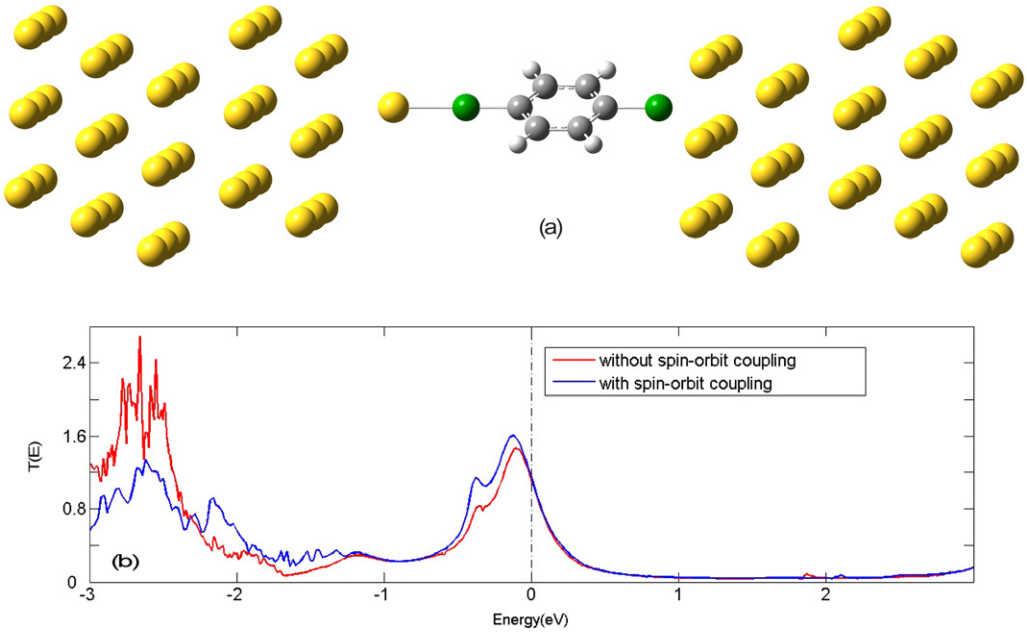

Figure 5. Transport calculations for a BDT molecule attached asymmetrically to two 3D Au electrodes at the Au (111) hollow site on one side and to a Au adatom on the other side: (a) optimized geometry; (b) SR and FR transmission coefficients.

composed from the HOMO-2, as shown in figure 3(e). In contrast the HOMO cannot interact with the $m = 0$ band of the Au monatomic chain, so that it contributes only with a very sharp transmission peak below E_F. The situation is different for FR calculations. In this case the wavefunctions of the Au electrodes at E_F also include the $5d_{yz}$ orbital besides the 6s and $5d_{z^2}$ ones. These interact strongly with the HOMO, so that it can contribute to the transmission at E_F. The corresponding conduction channel isosurface is given in figure 3(f).

We then conclude that in this 1D example the inclusion of SO coupling is rather important both from the qualitative and quantitative points of view. At the qualitative level, the conductance is limited in the SR case by the number of conduction channels in the electrodes, and in the FR case by the molecule–electrode coupling. At the quantitative level, SO coupling enhanced the transmission coefficient at E_F from 1.88 to 2.20.

3.4. BDT connected with 3D Au electrodes

Next we analyze the transport properties of a BDT molecule connected to two semi-infinite 3D Au electrodes. Here, we consider three types of contact configurations. In the first one BDT is symmetrically attached to the hollow site of the two Au (111) surfaces (see figure 4(a)), and the distance between the S atom and the plane of the gold surface is optimized to be 1.90 Å [37]. The transmission coefficients are shown in figure 4(b) for both SR and FR calculations. Clearly, for this junction the SO coupling only slightly affects the overall transport properties, and especially at the Fermi level the transmission coefficient is the same regardless of the SO interaction. This can be easily understood, by recalling that SO does not change either the frontier molecular orbitals of BDT or the band structures of bulk Au around E_F by very much.

In the second binding configuration BDT is asymmetrically attached to two Au (111) surfaces, namely at the (111) hollow site on one side and to an adatom on the other side (see figure 5(a)). Here, the distance between S and the plane of the Au surface is kept at 1.90 Å at the hollow site, while the distance between S and the Au adatom is optimized to be 2.39 Å [37]. The transmission coefficients as a function of energy for this junction are shown in figure 5(b). Although the FR transmission almost perfectly follows the SR transmission above the Fermi level, below E_F the effects of SO interaction become more substantial. The transmission peak just below E_F is increased by about 14.3%, and the shoulder at slighter lower energies becomes more pronounced, indicating that SO coupling causes splitting of molecular orbitals due to the presence the Au adatom.

Finally in the third configuration BDT is symmetrically attached to Au adatoms at both the Au (111) surfaces of the electrodes (see figure 6(a)). Here the distance between the S and the terminating adatom is the same as that in figure 5(a). In contrast to the previous two junctions, the inclusion of SO coupling now has a significant influence on the transmission, as one can see from figure 6(b). Clearly, the SO coupling significantly affects the transmission in the energy range from -1.80 eV to -3.0 eV. For example, the peak centers of the double-peak structure are located at -2.56 eV and -2.32 eV in the SR case, but they move to -2.64 eV and -2.22 eV in the FR one. Such a shift can be traced back to the modifications of the band structure of bulk Au due to SO coupling. In fact, as one can see in figure 1(b), it is the energy range from -1.8 eV to -6.0 eV where SO coupling modifies the band structure of bulk gold significantly.

However for this bonding geometry also around E_F, the SO coupling affects the junction transmission. The relative changes in transmission generated by SO coupling can be

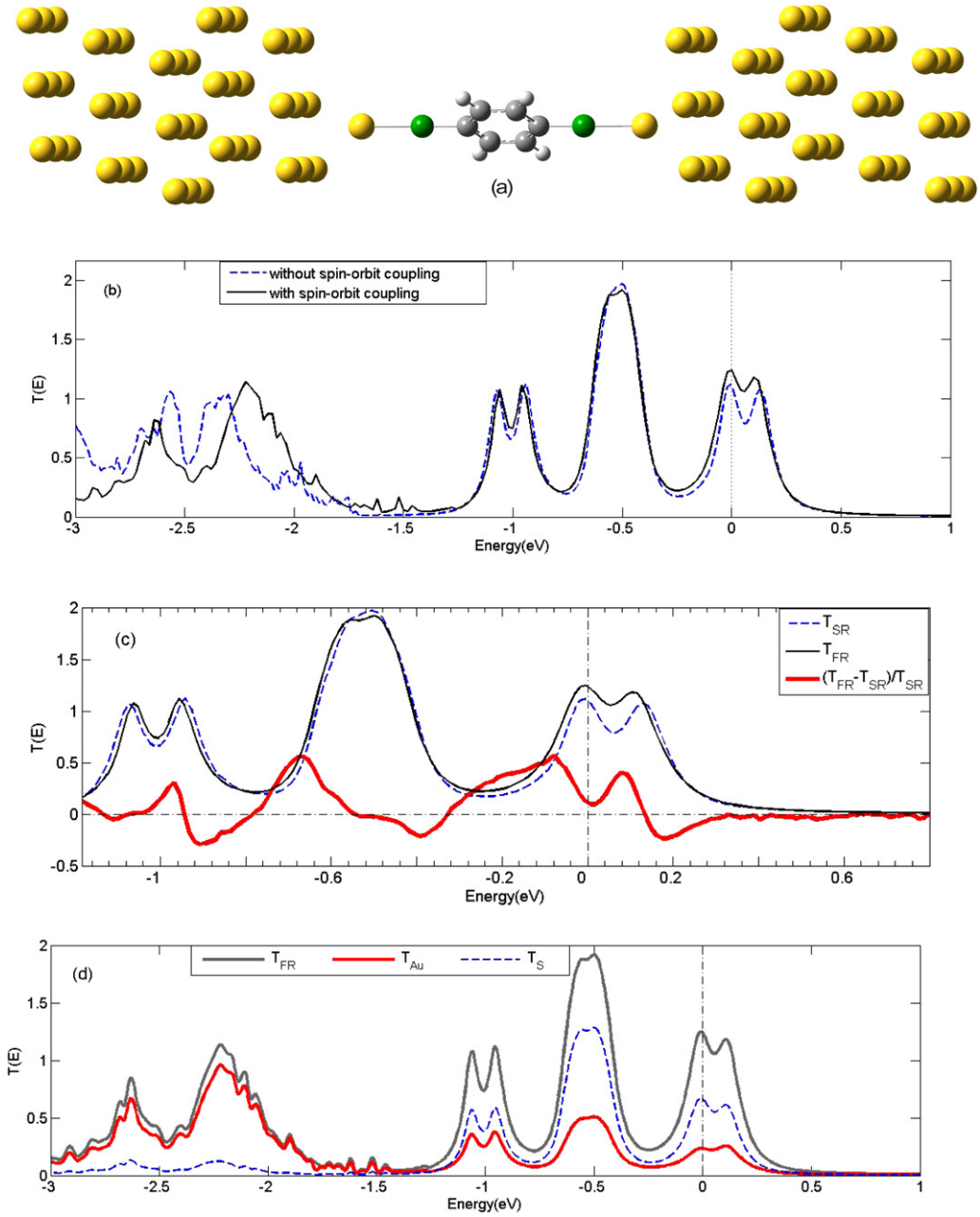

Figure 6. Transport calculations for a BDT molecule attached to two 3D Au electrodes at Au adatoms: (a) optimized geometry; (b) SR and FR transmission coefficients; (c) $(T_{\mathrm{FR}} - T_{\mathrm{SR}})/T_{\mathrm{SR}}$ as a function of energy; (d) projected transmission coefficient onto the Au adatoms and the S atoms of the thiol groups.

quantified by the quantity $(T_{\mathrm{FR}} - T_{\mathrm{SR}})/T_{\mathrm{SR}}$. This is the difference between the transmission coefficient calculated by using the FR, T_{FR}, and that calculated by using the SR corrections, T_{SR}, and normalized by T_{SR}. This quantity is plotted in figure 6(c) where one can observe modifications as large as 50% in the energy range $[-1.0, 0.4]$ eV. These changes persist at the Fermi level where the transmission coefficient is increased from 1.09 (SR case) to 1.24 (FR case), a net change of 13.8%.

Projected transmission analysis shows that the two gold adatoms play a crucial role in the transmission of the junction, as presented in figure 6(d). For the specific double-peak structure at the Fermi level, the LUMO and the LUMO + 1 state of the central $C_6H_4S_2Au_2$ molecule make the main contributions for both the SR and FR calculations. Although SO coupling does not split molecular orbitals further, it does change the separation among the frontier molecular orbitals of the $C_6H_4S_2Au_2$ molecule. For instance, the gap between LUMO and LUMO + 1 is decreased from 0.20 eV in the SR case to 0.17 eV in the FR case. This is the main reason for the increase of the transmission coefficient at the Fermi level.

An interesting final question is why the SO coupling affects the conductance so differently in Au quantum point contacts as compared to BDT junctions bridged with adatoms

on both sides of the junction. Such a difference is rooted in two main factors, namely the spacing among the relevant molecular orbitals, and the coupling strength between the central molecule (Au_3 and $C_6H_4S_2Au_2$) and the electrodes. For Au_3, the SO coupling does cause the splitting of the molecular orbitals. However the energy levels of the frontier molecular orbitals are very dense, with a spacing of the order of 0.03 eV. Furthermore the coupling between Au_3 and the two gold electrodes is very strong and the SO interaction does not change the bonding nature of the frontier molecular orbitals. Therefore, for all these reasons the SO coupling cannot affect the low-bias conductance of the gold quantum point contact (at least for short chains). In contrast the picture is totally different for $C_6H_4S_2Au_2$. In this case the separation among the frontier molecular orbitals is rather large (for example the LUMO + 1 is about 0.17 eV higher than the LUMO). The coupling between $C_6H_4S_2Au_2$ and the electrodes is relatively weak, as it can be clearly deduced from the sharp peaks appearing in the transmission plot. Thus, the energy shift and the broadening caused by the interaction between $C_6H_4S_2Au_2$ and the electrodes are small and the effects arising from the SO-induced modification of the electronic structure of the $C_6H_4S_2Au_2$ molecule are magnified.

4. Conclusion

In this paper we use BDT as a benchmark molecule to study the influence of SO interaction over the electronic transport properties of molecular devices contacted to Au electrodes. In general we find that the effects of SO interaction are more pronounced in devices with electrodes having reduced symmetry, where the modification of the electrode band structure due to SO are magnified. In contrast, the transmission in devices made by 3D electrodes is less sensitive to the SO corrections to the band structure although, even in this case, changes in the low-bias transmission up to 13% can be found for geometries where the molecule is only weakly bound to the electrodes.

Acknowledgments

The authors (R Li and S Hou) thank Professor Wenjian Liu for the helpful discussion on relativistic density functional theory. Dr Toher, who is kindly acknowledged, has provided the atomic coordinates used in this work. This project was supported by the National Natural Science Foundation of China (No. 60771002), the MOST of China (Nos 2006CB932404 and 2007CB936204) and the Ministry of Education of China (NCET-07-0014). The Smeagol project (SS) is sponsored by the Science Foundation of Ireland.

References

[1] Nitzan A and Ratner M A 2003 *Science* **300** 1384
[2] Tao N J 2006 *Nat. Nanotechnol.* **1** 173
[3] Reed M A, Zhou C, Miller C J, Burgin T P and Tour J M 1997 *Science* **278** 252
[4] Xiao X, Xu B and Tao N J 2004 *Nano Lett.* **4** 267
[5] Lörtscher E, Weber H B and Riel H 2007 *Phys. Rev. Lett.* **98** 176807
[6] Xu B and Tao N J 2003 *Science* **301** 1221
[7] Venkataraman L, Klare J E, Tam I W, Nuckolls C, Hybertsen M S and Steigerwald M L 2006 *Nano Lett.* **6** 458
[8] Ulrich J, Esrail D, Pontius W, Venkataraman L, Millar D and Doerrer L H 2006 *J. Phys. Chem.* B **110** 2462
[9] Chen F, Li X, Hihath J, Huang Z and Tao N J 2006 *J. Am. Chem. Soc.* **128** 15874
[10] Meir Y and Wingreen N S 1992 *Phys. Rev. Lett.* **68** 2512
[11] Thygesen K S 2006 *Phys. Rev.* B **73** 035309
[12] Hohenberg P and Kohn W 1964 *Phys. Rev.* **136** B864
[13] Kohn W and Sham L J 1965 *Phys. Rev.* **140** A1133
[14] Zhang J, Hou S, Li R, Qian Z, Han R, Shen Z, Zhao X and Xue Z 2005 *Nanotechnology* **16** 3057
[15] Xue Y, Datta S and Ratner M A 2002 *Chem. Phys.* **281** 151
[16] Ke S-H, Baranger H U and Yang W 2004 *Phys. Rev.* B **70** 085410
[17] Taylor J, Guo H and Wang J 2001 *Phys. Rev.* B **63** 245407
[18] Brandbyge M, Mozos J-L, Ordejón P, Taylor J and Stokbro K 2002 *Phys. Rev.* B **65** 165401
[19] Rocha A R, García-Suárez V M, Bailey S, Lambert C, Ferrer J and Sanvito S 2006 *Phys. Rev.* B **73** 085414
[20] Rusakov A A, Rykova E, Scuseria G E and Zaitsevskii A 2007 *J. Chem. Phys.* **127** 164322
[21] Nautiyal T, Youn S J and Kim K S 2003 *Phys. Rev.* B **68** 033407
[22] Corso A D, Smogunov A and Tosatti E 2006 *Phys. Rev.* B **74** 045429
[23] Hall L E, Reimers J R, Hush N S and Silverbrook K 2000 *J. Chem. Phys.* **112** 1510
[24] Lu W and Lieber C M 2007 *Nat. Mater.* **6** 841
[25] Ohnishi H, Kondo Y and Takayanagi K 1998 *Nature* **395** 780
[26] Thijssen W H A, Marjenburgh D, Bremmer R H and van Ruitenbeek J M 2006 *Phys. Rev. Lett.* **96** 026806
[27] Nazin G V, Qiu X H and Ho W 2003 *Science* **302** 77
[28] Qian Z, Li R, Hou S, Xue Z and Sanvito S 2007 *J. Chem. Phys.* **127** 194710
[29] Crljen Ž and Baranović G 2007 *Phys. Rev. Lett.* **98** 116801
[30] Qian Z, Li R, Zhao X, Hou S and Sanvito S 2008 *Phys. Rev.* B **78** 113301
[31] Li R, Zhang J, Hou S, Qian Z, Shen Z, Zhao X and Xue Z 2007 *Chem. Phys.* **336** 127
[32] Fernandez-Seivane L, Oliveira M A, Sanvito S and Ferrer J 2006 *J. Phys.: Condens. Matter* **18** 7999
[33] Soler J M, Artacho E, Gale J D, García A, Junquera J, Ordejón P and Sánchez-Portal D 2002 *J. Phys.: Condens. Matter* **14** 2745
[34] Perdew J P and Zunger A 1981 *Phys. Rev.* B **23** 5048
[35] Toher C, Filippetti A, Sanvito S and Burke K 2005 *Phys. Rev. Lett.* **95** 146402
[36] Toher C and Sanvito S 2007 *Phys. Rev. Lett.* **99** 056801
[37] Toher C and Sanvito S 2008 *Phys. Rev.* B **77** 155402
[38] Kleinman L 1980 *Phys. Rev.* B **21** 2630
[39] Bachelet G B and Schuter M 1982 *Phys. Rev.* B **25** 2103
[40] Kleinman L and Bylander D M 1982 *Phys. Rev. Lett.* **48** 1425
[41] Hou S, Li R, Qian Z, Zhang J, Shen Z, Zhao X and Xue Z 2005 *J. Phys. Chem.* A **109** 8356
[42] Corso A D and Conte A M 2005 *Phys. Rev.* B **71** 115106
[43] Li R, Hou S, Zhang J, Qian Z, Shen Z and Zhao X 2006 *J. Chem. Phys.* **125** 194113
[44] Di Ventra M, Pantelides S T and Lang N D 2000 *Phys. Rev. Lett.* **84** 979
[45] Xue Y and Ratner M A 2003 *Phys. Rev.* B **68** 115406
[46] Xue Y and Ratner M A 2003 *Phys. Rev.* B **68** 115407
[47] Basch H, Cohen R and Ratner M A 2005 *Nano Lett.* **5** 1668
[48] Andrews D Q, Cohen R, Van Duyne R P and Ratner M A 2006 *J. Chem. Phys.* **125** 174718
[49] Ke S-H, Baranger H U and Yang W 2007 *J. Chem. Phys.* **127** 144107
[50] Thygesen K S, Strange M, Kristensen I S and Jacobsen K W 2008 *J. Chem. Phys.* **128** 114714